

Proceedings of the ASME 2024 Conference on Smart Materials,
Adaptive Structures and Intelligent Systems
SMASIS2024
September 9-11, 2024, Atlanta, Georgia

## SMASIS2024-139944

## THE PHYSICS OF BIO-INSPIRED COVERT FLAPS AS FLIGHT CONTROL DEVICES

Diaa A. Zekry<sup>1,†,\*</sup>, Aimy A. Wissa<sup>1,†,\*</sup>,

<sup>1</sup>Princeton University, Princeton, NJ

### **ABSTRACT**

Covert-inspired flaps are novel feather-inspired aerodynamic control surfaces that enable stability augmentation and maneuvering in small-scale Uncrewed Aerial Vehicles (sUAVs), especially for tailless configurations. For the first time, this paper uses time-averaged particle image velocity (PIV) to reveal the effect of static covert-inspired flaps on the flow field when simultaneously deflected on a wing's upper (suction) and lower (pressure) surfaces. Compared to a flap deployed on a single side, the simultaneously deflected flaps enhance the modulation range of the aerodynamic response (i.e., lift, drag, and pitching moment), making them more effective as control surfaces. Results reveal two categories explaining why the modulation range of the simultaneous deflection response is larger than each side deflection alone. Limit-bounded cases, where the response is within the bounds of the single-sided experiments, and limit-expanding cases, where the interaction between the suction and pressure sides flaps is crucial. Limit-expanding cases are associated with flow fields with increased wake size or flow features that cannot be reconstructed from the suction-only or pressure-only flow fields. Using the velocity fields, we also show that superposition better predicts post-stall responses than pre-stall responses because the flow features present in the wake of the post-stall flow are similar between suction-only, pressure-only, and simultaneous deflection experiments. Finally, we show that the post-stall flow is more sensitive to pressure side flaps than suction side flaps due to significant flow changes occurring at the pressure side when the pressure side flap is deflected, which can increase the size of the wake and significantly alter the response. The results from the flow fields support the data-driven aerodynamic models that express the lift, drag, and pitching moment as a function of the flow and flap parameters.

# Keywords: covert-inspired flaps, bio-inspired flight control, feather-inspired flaps

Documentation for asmeconf.cls: Version 1.37, May 2, 2024.

### NOMENCLATURE

Free stream conditions

 $U_{\infty}$  Free stream air velocity [m/s]  $\rho_{\infty}$  free stream air density  $[kg/m^3]$  q dynamic pressure  $[N/m^2]$   $\alpha$  Angle of attack [rad or degree]

Wing geometry

c wing chord length [m]

b wing span [m]

S wing planform area  $[m^2]$ 

covert-inspired flap variables  $c_f$  flap chord length [%c]

 $\beta$  Covert-inspired flap deflection angle [rad or degree]

x Location of covert-inspired flap [%c]

Aerodynamic coefficients

Coefficient of lift [-]

 $C_d$  Coefficient of drag [-]

 $C_m$  Coefficient of pitching moment about quarter chord [-]

Other coefficients

 $R^2$  Coefficient of determination [-]

subscripts

 $()_s$  suction side variable

 $()_p$  pressure side variable

## 1. INTRODUCTION

Mission demands for Small-scale Uncrewed Aerial Vehicles (sUAVs) have increased in the past few decades. sUAVS are now used in a wide range of applications, ranging from surveillance and reconnaissance to firefighting. This diversity in missions and applications necessitates the design and use of various types of configurations of sUAVs. One such configuration is the Blended Wing Body (BWB)[1]. Due to their unconventional shape and aerodynamic characteristics, BWBs are often hard to stabilize and control. However, they have advantages, such as reduced drag and larger lifting surfaces, increasing the aircraft's efficiency and reducing its operational costs [2–5]. Thus, for BWB to meet the demands of a more extensive flight envelope, they require

<sup>†</sup>Joint first authors

<sup>\*</sup>Corresponding author: awissa@princeton.edu

high-performing control surfaces that can provide the necessary control authority throughout the whole flight regime.

Birds are the biological analogy to sUAVs, especially for some of the BWB configurations where the vertical stabilizer is not present, as they both fly at similar Reynolds number regimes, leading to similar control and stability challenges. However, unlike sUAVs, birds are agile and maneuverable. Birds rely on an integrated flow and flight control system to modulate the surrounding flow at small and large scales and maintain their flight performance during different maneuvers. Large-scale mechanisms include wing morphing, such as changes in the wing's sweep, dihedral, and planform shape[6–8]. While examples of small-scale mechanisms include the deployment of feathers systems, such as the coverts, alula, and wingtips [8, 9]. Covert feathers are the concentration of this paper.

Coverts are groups of feathers that outline a bird's wing. They are present on both the upper and lower surfaces of the wing. Coverts are divided into primaries covering the hand wing and secondaries covering the arm wing. Secondary coverts are further categorized based on their location along the chord. For example, leading Edge (LE) coverts are named the lesser coverts, while intermediate and trailing Edge (TE) coverts are referred to as median, and greater coverts, respectively (figure 1) [8–11].

Carruthers et al. [8] recorded the deployment of the covert feathers on steppe eagles *Aquila nipalensis* during flight. They observed that the upper and lower side coverts are usually deployed simultaneously during different flight maneuvers. Despite the simultaneous deployment observations, covert-inspired structures have been mainly studied on the suction side alone [12–21], and on the pressure side alone [19].

Recently, Zekry et al. [22] studied the simultaneous deflection of covert-inspired flaps on the suction and pressure sides of a two-dimensional wing. In that study, the authors show that the simultaneous deflection of the covert-inspired flaps has a wider range of aerodynamic force and moment modulation than single-sided deflections, suggesting that deploying the covertinspired flaps on both the suction and pressure sides makes them more effective as flight control devices for BWB configurations, compared to a single side. Further, aerodynamic models show the sensitivities of the aerodynamic response, namely lift, drag, and pitching moment, to the location and deflection angle of the covert-inspired flap, vary between the pre and post-stall regimes. However, the pressure side flap parameters were more dominant during post-stall. Moreover, the authors describe a superposition principle that uses information from the pressure side and suction side to predict the behavior of the simultaneous deflection experiment. Results show that superposition only works in a limited flight regime and predominantly at post-stall angles of attack. The study relates their findings to Carruthers's [8] flight observations, emphasizing the importance of simultaneous covert deflection for specific maneuvers.

However, Zekry et al. [22] work does not explain the physical mechanisms of the simultaneous covert deflection and how they compare to a single-sided flap, which is the focus of this paper. In this paper, we develop an understanding of the flow physics that describes the covert-inspired flaps as flight control effectors using time-averaged Particle Image Velocimetry (PIV).



FIGURE 1: Covert feathers highlighted on the pressure side of a bird's wing. PC: primary coverts, SLC: secondary lesser coverts, SMC: secondary marginal coverts, SGC: secondary greater coverts. This figure and naming conventions are adapted from [8, 22]. The images have been obtained by the author(s) from the Pixabay website, where they were made available under the Pixabay License. It is included within this article on that basis.

More specifically, we answer these three questions:

- 1. Why does the simultaneous deployment of covert-inspired flaps have a larger modulation range of the aerodynamic forces and moments compared to single-sided deflection?
- 2. Why are the aerodynamic responses more sensitive to pressure side variables than suction side variables in post-stall conditions?
- 3. Why is the superposition concept more applicable to the post-stall regime than the pre-stall regime?

The rest of the paper is divided into three sections. The background section recaps some of the results from Zekry et al. [22] to contextualize this paper's results. The methods section describes the wind tunnel experimental techniques and the PIV procedures. Finally, the results and discussion section presents the findings in three subsections to answer each of the research questions mentioned above.

## 2. BACKGROUND

## 2.1 Nature flight observations

Carruthers et al. [8] used high-speed video footage from a camera carried by the birds (*Aquila nipalensis*) to study the deployment behavior of wing feathers during different maneuvers. The authors report four main observations that are relevant to the current work.

- 1. Most landing and perching maneuvers include underwing lesser covert deflection
- 2. Underwing lesser coverts are often deployed towards the end of the pitch-up phase of the perching maneuver

- The deployment of underwing coverts was frequently accompanied by upperwing covert deflection and alula protraction.
- 4. Upperwing greater coverts deploy during gust encounters

## 2.2 Engineering system experimental observations

Zekry et al. [22] explored the role of simultaneously deflecting covert-inspired flaps on a two-dimensional wing. The key takeaways of the study are related to 1) the effect of simultaneously deflecting covert-inspired flaps on the pressure and suction sides of an airfoil on the aerodynamic response, namely, lift, drag, and pitching moment compared to single-sided deflection, 2) the sensitivity of the aerodynamic response to the flaps' location and deflection angle, and 3) the possibility of reconstructing the two-sided flap response from the single flap response.

**2.2.1 Modulation range.** Zekry et al. [22] used a closed-loop wind tunnel facility to measure the aerodynamic forces and moments over a 2D NACA 2414 airfoil at a Reynolds number (Re) of 200,000. They split their aerodynamic characterization results into pre- and post-stall, showing the main effect plots for both regimes. An adaptation of their pre-stall lift results is shown in figure 2, where each subplot has either a red line or a blue line corresponding to the pressure-only or suction-only experiments, respectively. The simultaneous deflection is shown using a black line. Each of the lines has a shaded region corresponding to the achievable response limits of the response for each experiment.

Figure 2 clearly shows the increase in the area of the shaded grey region corresponding to the simultaneous deflection experiment compared to each of the red and blue regions, corresponding to each side alone. These observations are similar to the other responses (i.e., drag and pitching moment) and both the pre-stall and post-stall AoA regimes.

**2.2.2 Parameter sensitivity.** Main effect plots also show the sensitivity of each response to each input parameter through the slope of the mean line. For example, Figure 2 shows that the pre-stall lift for the simultaneous deflection case is, by average, more sensitive to the pressure side location  $x_p$ , and the suction side deflection angle  $\beta_s$  compared to the other parameters. Zekry et al. [22] further confirmed this sensitivity using a data-driven model based on analysis of variance. A sample output equation 1 is shown for the pre-stall lift of the simultaneous deflection case.

$$\begin{split} preC_{l_{2sides}} &= 0.273 + [578.0\beta_p - 3980.0\alpha - 1330.0\beta_s + 420.0x_p \\ &- 584.0x_s - 37.1\alpha\beta_p + 54.7\alpha x_p + 81.3\alpha x_s - 5.22\beta_p\beta_s \\ &+ 9.1\beta_p x_p - 6.8\beta_s x_p + 195.0\alpha^2 + 10.7\beta_s^2] \times 10^{-5} \\ R_{adj_{model}}^2 &= 95.11\% - R_{adj_{validation}}^2 = 90.36\% \quad (1) \end{split}$$

where  $C_l$  is the coefficient of lift,  $\alpha$  is the angle of attack,  $x_s$  and  $x_p$  are the suction and pressure covert location as a percent of the chord, respectively, and  $\beta_s$  and  $\beta_p$  are the suction and pressure covert deflection angles, respectively.

Table 1 shows the parameters most effective at modulating the aerodynamic responses for the simultaneous deflection cases in the pre and post-stall lift regimes. Generally, for pre-stall,

TABLE 1: Parameters with the highest sensitivity for aerodynamic responses

Regime	Lift	Drag	Pitching Moment
Pre-stall Post-stall	$x_p, \beta_s$ $x_p$	$\beta_p, \beta_s$ $x_p, \beta_p$	$x_p, x_s$ $x_p$

TABLE 2: Coefficient of determination  $R^2\%$  of the superposition principle

Regime	Lift	Drag	Pitching Moment
Pre-stall	75%	68%	95%
Post-stall	87%	95%	93%

the lift is more affected by the suction side parameters, drag by deflection angles, and pitching moment by the flap location. For post-stall, the pressure side flap significantly affects all the responses.

**2.2.3 Concept of superposition.** Zekry et al. [22] use their data-driven models to show interactions between the pressure and suction side coverts. For example, in equation 1, second-order terms like  $\beta_s\beta_p$  and  $\beta_sx_p$  are statistically significant interaction terms between the suction and pressure sides that affect the pre-stall lift for the simultaneous deflection cases. To understand the importance of the interactions, the authors introduced the concept of superposition to explore using suction-only and pressure-only experiments in predicting the simultaneous deflection results. The results show that superposition works in most of the cases. However, it can only predict 75% of pre-stall lift and 68% of pre-stall drag as indicated by table 2.

While Carruthers et al. [8] reported on flight observations, and Zekry et al. [22] focused on aerodynamic models, the physics governing the simultaneous deflection of coverts and covert-inspired flaps is still needed. In the following sections, we will use PIV to answer the questions posed in the introduction and relate our findings to the observations from Carruthers et al. [8] and Zekry et al. [22].

## 3. METHODS

Experiments were conducted at Princeton's closed-loop closed test section wind tunnel shown in figure 3. The wind tunnel is a low-speed, low-turbulence tunnel with three test sections, each measuring 1.2m by 1.2m by 1m. The experiments were performed in the third test section. The wing was mounted on one side to an ATI Gamma 6-axis force-torque transducer to measure the aerodynamic forces and moments. On the other end of the wing, an acrylic splitter plate was placed to approximate two-dimensional flow around the airfoil [23]. The forces were sampled at 1kHz and the lift and drag forces were calculated by resolving the body force measurements into the wind axis. The pitching moment is reported around the approximate aerodynamic center at the quarter chord position. All reported responses were non-dimensionalized according to convention using dynamic pressure q, planform area S, and chord c, where  $q = \frac{1}{2}\rho_{\infty}U_{\infty}^2$  [24]. A Velmex B48 with a stepper motor was used

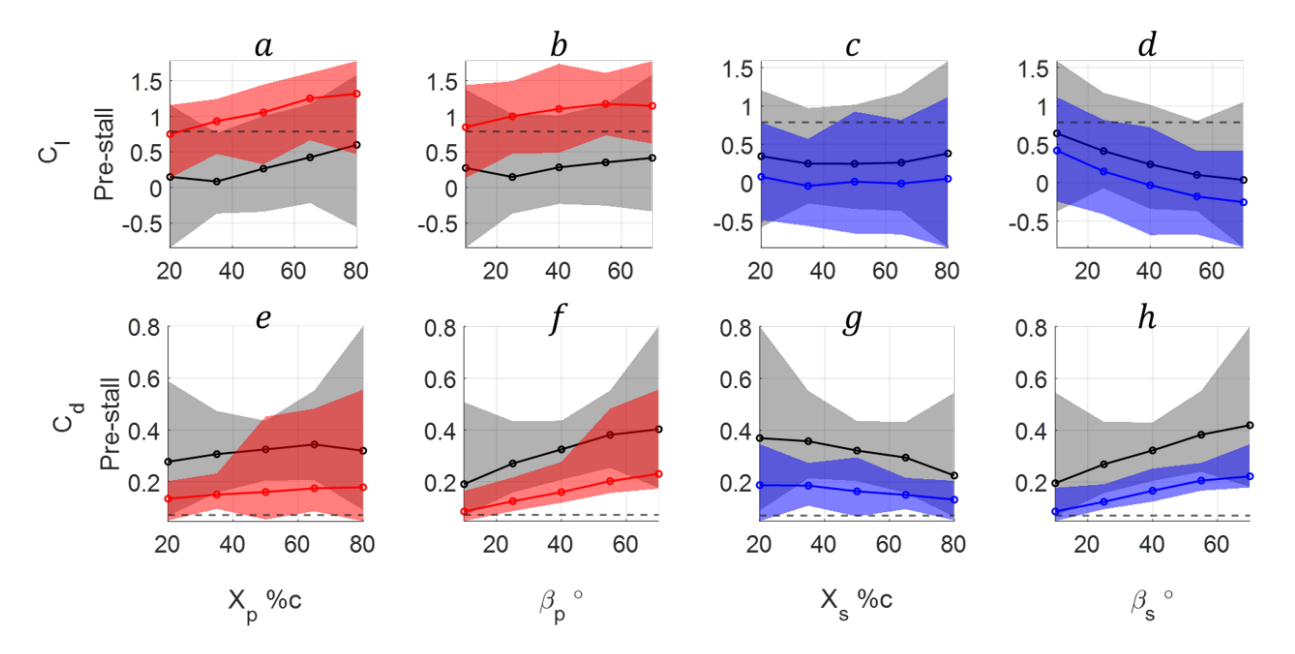


FIGURE 2: Main effect plots for pre-stall lift (upper row) and drag (lower row) for every design parameter. The baseline is depicted with a dashed black line. The pressure side is indicated in red, the suction side in blue, and simultaneous deflection in solid black. The colored regions illustrate the range of responses. Adapted from [22].

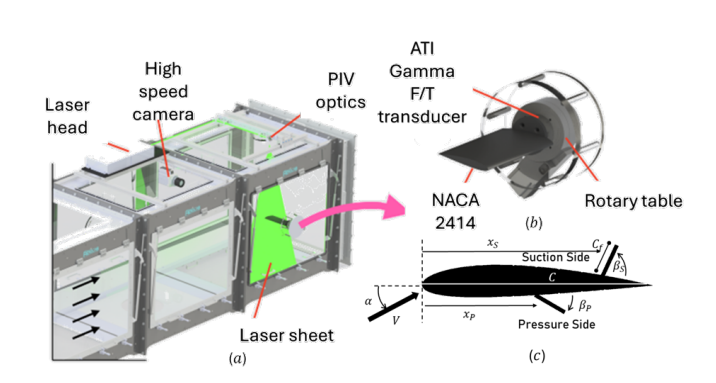


FIGURE 3: a) wind tunnel schematic with the PIV setup and laser sheet shown b) wing setup integrated with the ATI force transducer and the rotary table. c) airfoil schematic showing the experimental parameters

to vary the AoA with an accuracy of  $0.0125^{\circ}$ . The free-stream conditions were set to  $U_{\infty} = 26m/s$ , corresponding to a Re of 200,000, to match previous studies [12, 22, 25]. Blockage effects were considered and accounted for using solid and wake blockage equations [23].

Planer PIV was used to attain time-averaged flow field measurements around the wing. The PIV measurements are acquired at a rate of 1kHz, using a Photonics DMX high-speed Nd:YLF 527nm dual cavity high-repetition laser. A series of  $90^{\circ}$  mirrors was used to redirect the laser beam to the area of interest, and a series of converging and diverging lenses were used to change the beam's width and focal length such that the focal point of the sheet lies in the center of the region of interest with a thickness less than 2mm. The laser beam is fanned out into a sheet using a -10mm cylindrical lens. Neutrally buoyant Di-Ethyl-Hexyl-Sebacat (DEHS) particles with an average diameter of  $5\mu m$  were used for seeding.

Image pairs were taken using a 9MP Photron Nova R5 high-speed CMOS camera. The acquired images were processed using multi-pass cross-correlation in LaVision's DaVis software. A  $64\times64px$  square interrogation window was used for the first three correlation passes, and a  $24\times24px$  adaptive interrogation window was used for the following three passes. The interrogation regions were overlapped by 50%. A median universal outlier filter with a  $5\times5$  filter region was used for all cases. The final vector spaces presented are time-averaged flow fields for 120 frames corresponding to 0.12s, which was shown to be representative of the average flow field.

The wing model was 3D printed using rigid 10K material on an SLA Form 3 printer. To match previous studies, the wing cross-

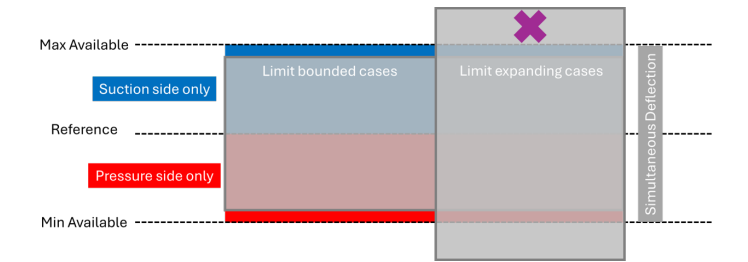


FIGURE 4: A schematic comparing the range of modulation of the responses for three experiments: suction side only (blue), pressure side only (red), and simultaneous deflection (grey). There are two categories for the simultaneous deflection experiment: The limit-bounded cases are bounded by the red and blue, and the limit-expanding cases are where the response extends beyond the limits available by red and blue. The purple "X" shows a limit example of a limit expanding case that is discussed in the results

section was a NACA 2414 with a rectangular planform that had a chord, c = 0.120m, and a span, b = 0.280m. The covert-inspired flaps had a rectangular cross-section with a length covering the whole wing span, a chord length,  $c_f = 20\%c$ , and a thickness of 2mm. For each configuration tested, the flap was static. The flap location was fixed using clear tape, and the deflection angle was set using a small triangular wedge between the flap and the wing.

Three experiments were conducted: suction side only, pressure side only, and simultaneous deflection. For each of the experiments, five parameters were varied. These are the AoA  $\alpha$ , covert-inspired flap location on the suction and pressure sides  $x_s$ , and  $x_p$ , respectively, and the flap deflection angles on the suction and pressure sides,  $\beta_s$ , and  $\beta_p$ , respectively. The pressure side flap was removed entirely for the suction-only experiment and vice versa for the pressure-only experiment.

## 4. RESULTS AND DISCUSSION

## 4.1 Modulation range

The simultaneous deflection of the control surfaces expands the modulation range of the aerodynamic responses through two distinct mechanisms when compared to suction-only or pressureonly experiments. The first is referred to as the limit-bounded cases, while the second is referred to as limit-expanding cases.

The limit-bounded cases in figure 4 are where the limit of the available control authority is set by either deploying the suction side covert alone or the pressure side covert alone. While the simultaneous deployment for this case does not produce any additional control authority, it has access to a larger range. Assuming the coverts do not affect the flow/wing geometry when stowed, the simultaneous deflection has access to the full range of the suction-only responses when the pressure side covert is stowed, and similarly for the pressure-only responses when the suction side covert is stowed. Additionally, all intermediate response values inside the area can be achieved using different combinations of suction and pressure deflection angles, which increases the area of the box in figure 4 and effectively doubles the available control authority.

When examining the pre-stall lift results, all the configurations represent limit-bounded cases. Figure 2 shows that the pressure side area (red) (figure 2a at  $x_p = 40\%c$ ) covers regions that reach a maximum higher than the simultaneous deflection area (grey), indicating that a pure pressure side deflection can lead to a higher lift modulation. Similarly, pure suction deflections can achieve a lower minimum than simultaneous deflections (figure 2c at  $x_s = 40\%c$ ). Despite each side alone having a larger extreme compared to the simultaneous deflection, the area between the maximum and minimum is the largest for the simultaneous deflection (grey area figure 2), proving a wider modulation range for the limit-bounded cases (figure 4).

The limit-expanding cases (figure 4) are cases where the simultaneous deflection of the flaps extends the response beyond the limits of each side alone. These extensions are primarily due to interactions between the pressure and suction side coverts. For example, some flap configurations represent limit-expanding cases when examining the pre-stall drag response. Figure 2 shows that the pressure side area (red)(figure2e at  $x_p = 20\%c$ ) and the suction side area (blue)(figure2g at  $x_s = 20\%c$ ) have a maximum coefficient of drag that is less than that of the simultaneous deflection (grey).

PIV measurements can provide insight into the physics distinguishing limit-bounded and limit-expanding cases. Figure 5 shows the velocity magnitude of the flow field around the wing for pre-stall (upper row) and post-stall (lower row) for the suction-side (a,e), pressure-side (b,f), and simultaneous deflection experiments (c,g). Additionally, figure 5d and h are reconstructed flow fields created by superimposing the velocity fields of the pressure side of the pressure-only and suction side of the suction-only experiments into one image. The dashed lines indicate the limits of the wake size for each case.

For a limit-bounded case (i.e., the lower row of Figure 5), the limit lines 5 and 6 do not change between suction- and pressureonly, and the simultaneous deflection. Further, the superposition flow field is very similar to the simultaneous deflection flow field, indicating that the drag response is similar, also shown by Zekry et al. [22]. In contrast, for a limit-expanding case (i.e., the upper row of Figure 5), the limit lines 2 and 3 indicating the suctiononly and pressure-only wake boundaries are now shifted to lines 1 and 4 for the simultaneous deflection experiment, increasing the size of the wake. Also note that the area inside the white box (figure 5c,d) has a lower velocity for the simultaneous deflection, indicating that there is an interaction between the pressure and suction side flaps. For this specific case, the interaction is the elimination of the TE separation point, leading to an increased wake area behind the wing, which increases the pressure drag, prompting the total drag increase, as seen in the main effect plots (Figure 2e,f,g,h). The vanishing of the TE separation point is not due to the suction alone or pressure alone; instead, it was made possible due to the interaction of the simultaneously deflected flaps.

The classification between the two categories of cases is not absolute for all responses; rather, the classification of a case as a limit-bounded or limit-expanding depends on the response of interest. For example, by investigating the velocity field behind the airfoil, as marked by the white boxes (figure 5c, and d), the superposition does not match the measured flow inside the wake, which indicates that the pre-stall drag for the configuration

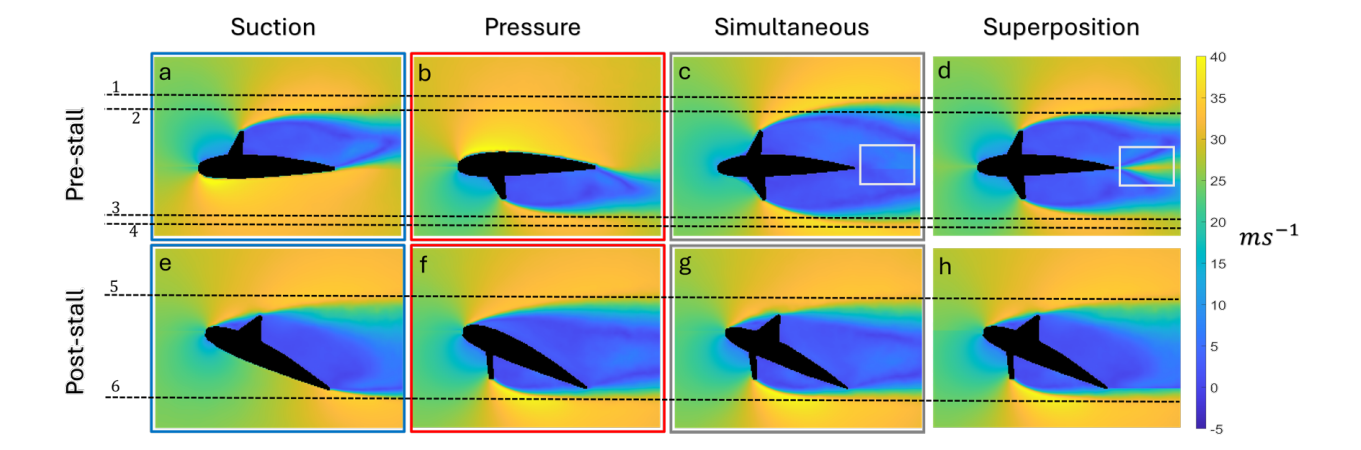


FIGURE 5: PIV velocity field for suction only (a,e), pressure only (b,f), simultaneous (c,g), and superposition (d,h) experiments. All velocity fields are measured except d and h, which are reconstructed from the suction side of a and e, superimposed to the pressure side of b and f, respectively. The dashed lines 1 through 6 indicate the limits of the wake for the different cases, and the white box highlights the difference in the wake between the simultaneous measured flow field and the superposition flow field

 $x_s = x_p = 20\%$  is considered a limit-expanding case. While for the same configuration, the velocity distribution directly above the airfoil surfaces is similar between Figures 5 c and d indicating that the pre-stall lift for the configuration  $x_s = x_p = 20\%$  is considered a limit-bounded case. This is further evident in Figure 2a,c,e,g) at  $x_s = x_p = 20\%$ , where the grey area extends beyond the red and blue area for  $C_d$  and is limited between the bounds of the red and blue for  $C_I$ .

## 4.2 Parameter sensitivity

According to the models in Zekry et al. [22], the post-stall response is modeled by functions of all experimental parameters. However, the response is most sensitive to the pressure side variables  $x_p$ , and  $\beta_p$ . To explain why, consider figure 6 where the velocity magnitude of the flow field around the wing is shown for the baseline a, suction side covert (b, c, d), and pressure side covert (e, f, g). For this post-stall angle of attack, the flow is completely separated on the suction side of the wing. A flap deflected on the suction side (figure 6c, d, and e) in this condition is always inside the shear layer for an averaged flow field, meaning that the wake size is, by average, not significantly different from that of the baseline (figure 6a). Similarly, the pressure side velocity is not different for figure 6c, d, and e compared to the baseline (figure 6a) because the suction side flaps do not significantly affect the flow on the pressure side. Therefore the velocity distribution on the suction and pressure side of figure 6b,c,d does not change significantly regardless of the location or deflection angle of the covert-inspired flap. Therefore, the sensitivity of the responses  $C_l$ ,  $C_d$ , and  $C_m$  to changes in the suction side variables is low.

To show the sensitivity of the response to the pressure side parameters, consider figure 6e, f, and g. The flow over the suction side between these three cases is similar. However, a pressure side flap causes a separation region behind the pressure side flap, which may or may not combine with the separated wake on the suction side of the wing. The location of the pressure side flap and its deflection angle are the dominant factors determining the

wake's final shape and pressure distribution around the wing. Hence, any small changes to  $x_p$  and  $\beta_p$  significantly change the responses, making the sensitivity of the responses  $C_l$ ,  $C_d$ , and  $C_m$  to changes in the pressure side variables high. Which makes the post-stall responses more sensitive to the pressure side coefficients than the suction side coefficients.

## 4.3 Concept of superposition

Superposition, as introduced by Zekry et al. [22], refers to the prediction of the simultaneous deflection responses using information exclusively from the suction-only and pressure-only experiments. The authors showed that, on average, superposition predicts responses better for post-stall than the pre-stall. Figure 5 shows the velocity magnitude of the flow field around the wing for pre-stall (upper row) and post-stall (lower row) for the suction only (a,e), pressure only (b,f), and simultaneous deflection (c,g) flow measurements. Additionally, figure 5d, and h is a constructed flow created by superimposing the velocity fields of the pressure side of the pressure-only and suction side of the suction-only experiments into one image. If the superposition holds, then figure 5c should match 5d, and similarly 5g should match 5h.

In pre-stall, the covert's deflection causes flow separation, with a slow-moving flow behind the flap in the wake. The separation points for single-sided deflections are at the flap and the TE. As for simultaneous deflection, the separation points are at the suction and pressure flaps, with the TE separation point eliminated. As mentioned in the previous section, the wake size in the simultaneous deflection is larger than the sum of the pressure-only and suction-only. Additionally, the wake of the superimposed flow is aphysical because of the source-like structure at the airfoil's LE and TE. The lack of this extra induced flow in the simultaneous deflection means that the measured flow in figure 5c cannot be predicted entirely from the information of the pressure-only or suction-only fields because figure 5c has extra information that both 5a, and b do not physically have. Hence, data-driven models based on suction-only and pressure-only data are limited

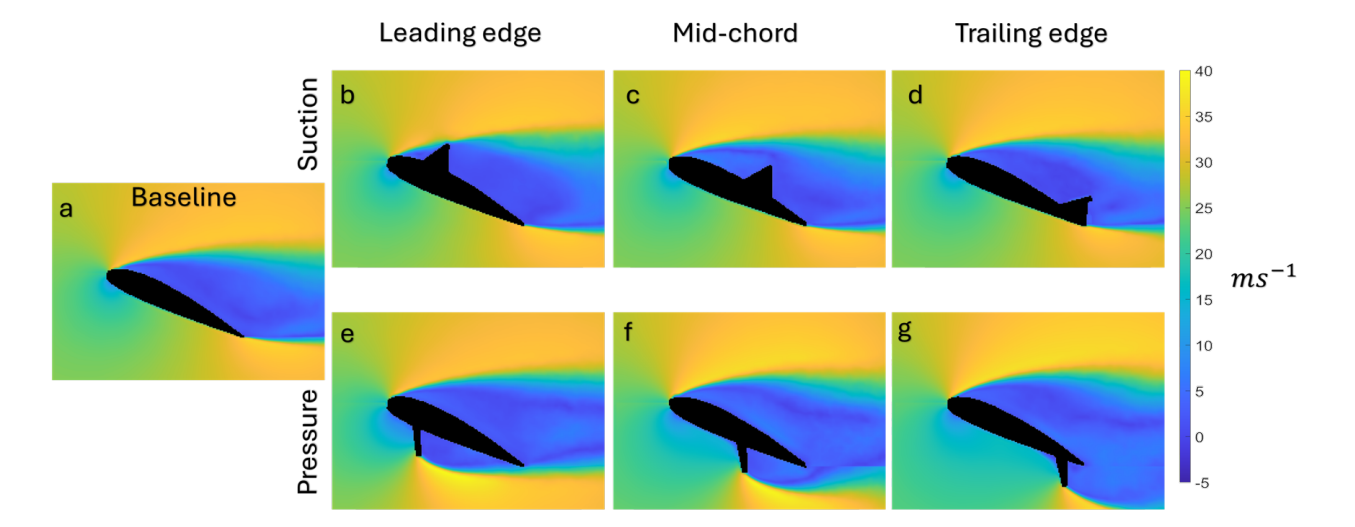


FIGURE 6: PIV velocity fields at AoA = 25° for a) baseline b)  $x_s = 20\% - \beta_s = 60^\circ$  c)  $x_s = 50\% - \beta_s = 60^\circ$  d)  $x_s = 80\% - \beta_s = 60^\circ$  e)  $x_p = 20\% - \beta_p = 60^\circ$  f)  $x_p = 50\% - \beta_p = 60^\circ$  g)  $x_p = 80\% - \beta_p = 60^\circ$ 

in their prediction capability of the simultaneous deflection.

On the other hand, in post-stall, the suction side separation point is near the LE, with the suction side covert inside the separated wake. Hence, the suction side flow properties are not significantly affected between the four cases shown in figure 5e, f, g, and h. Moreover, the pressure side flap deflection causes a separated flow behind the flap that is convected to merge with the wake of the suction side at the TE point. This means that the pressure side image 5f has similar physical features compared to the simultaneous deflection (figure5g). Further, the simultaneous deflection flow does not have extra flow features compared to the superpositioned flow (figure5h), which leads to stronger superposition data-driven models for post-stall cases because all the data needed to reconstruct the simultaneous deflection flow can be found in the pressure-only or suction-only experiments.

## 5. CONCLUSION

Covert-inspired flaps are superior flight control devices for sUAVs whose operational principles were previously poorly understood in the literature. We used PIV on a 2D NACA 2414 airfoil to study the flow field around the airfoil as the covert flap was deployed for three experiments, namely, suction-only, pressure-only, and simultaneous deflection. This paper answers three main questions:

1. Why does the simultaneous deployment of covert-inspired flaps have a larger modulation range of the aerodynamic forces and moments compared to single-sided deflection?

Ans: A configuration can have one of two categories: limit-bounded and limit expanding. As the name suggests, the simultaneous deployment in the limit bounded is bounded to the pressure-only and suction-only limits. In this category, the simultaneous deployment cannot access any extra control authority compared to the single-sided deflections. On the other hand, the limit expanding category has suction side and pressure side interactions that lead to extra flow

features such as a bigger wake, which eventually induces a larger response than the suction-only and pressure-only deflections.

2. Why are the aerodynamic responses more sensitive to pressure side variables than suction side variables in post-stall conditions?

Ans: In the post-stall regime, the flow is shown to be completely separated on the suction side, which makes the suction side flap lie inside the shear layer. Any deployment of the flap inside the shear layer does not significantly change the separated time-averaged flow field. Hence, the response is not very sensitive to the suction side flap location or deflection angle. On the other hand, the pressure side flap was shown to change the flow field on the pressure side by creating a separated flow region, which can reattach before the TE or merge with the suction side wake. This means that the pressure side flap location and deflection angle can have significant flow field changes, which significantly change the aerodynamic response. Hence, the flow is more sensitive to pressure side flaps than suction side flaps in post-stall flow conditions.

3. Why is the superposition concept more applicable to the post-stall regime than the pre-stall regime?

Ans: We showed that in pre-stall the elimination of the TE separation point in the simultaneous deflection experiment compared to the pressure-only and suction-only leads to a bigger wake size for the simultaneous deflection. In addition to the increase in the wake size, the simultaneous deflection has extra flow field features, such as a slower flow behind the TE. This means that superposition can only be used to predict part of the flow. On the other hand, in post-stall, the flow field of the suction side does not change significantly between the three experiments and the pressure side of the

pressure only is similar to the pressure side of the simultaneous deflection. Hence, the superposition can be used to predict the simultaneous deflection using only information from the pressure-only and suction-only experiments.

The PIV flow fields in this paper are relevant to the covert-inspired flaps as flight control devices as they provide insight into the physical mechanism by which the flight control devices work. This helps in the design process and configuration choice for a given control system requirements. Future work includes wider variations in the design parameter space and 3D PIV experiments to study the covert-inspired flaps as applied on a real wing.

## **REFERENCES**

- [1] Wang, Kelei and Zhou, Zhou. "Aerodynamic design, analysis and validation of a small blended-wing-body unmanned aerial vehicle." *Aerospace* Vol. 9 No. 1 (2022): p. 36.
- [2] Liebeck, Robert H. "Design of the blended wing body subsonic transport." *Journal of aircraft* Vol. 41 No. 1 (2004): pp. 10–25.
- [3] Okonkwo, Paul and Smith, Howard. "Review of evolving trends in blended wing body aircraft design." *Progress in Aerospace Sciences* Vol. 82 (2016): pp. 1–23.
- [4] Lixin, WANG, Zhang, Ning, Hailiang, LIU and Ting, YUE. "Stability characteristics and airworthiness requirements of blended wing body aircraft with podded engines." *Chinese Journal of Aeronautics* Vol. 35 No. 6 (2022): pp. 77–86.
- [5] Bonet, John T, Schellenger, Harvey G, Rawdon, Blaine K, Elmer, Kevin R, Wakayama, Sean R, Brown, Derrell L and Guo, Yueping. "Environmentally responsible aviation (ERA) project-n+ 2 advanced vehicle concepts study and conceptual design of subscale test vehicle (STV) final report." Technical report no. 2011.
- [6] March, Andrew I, Bradley, Charles W and Garcia, Ephraim. "Aerodynamic properties of avian flight as a function of wing shape." *ASME International Mechanical Engineering Congress and Exposition*, Vol. 42193: pp. 955–963. 2005.
- [7] Thomas, Adrian LR. "On the aerodynamics of birds' tails." *Philosophical Transactions of the Royal Society of London. Series B: Biological Sciences* Vol. 340 No. 1294 (1993): pp. 361–380.
- [8] Carruthers, Anna C, Thomas, Adrian LR and Taylor, Graham K. "Automatic aeroelastic devices in the wings of a steppe eagle Aquila nipalensis." *Journal of Experimental Biology* Vol. 210 No. 23 (2007): pp. 4136–4149.
- [9] Othman, Ahmed K, Zekry, Diaa A, Saro-Cortes, Valeria, Lee, Kyung Jun "Paul" and Wissa, Aimy A. "Aerial and aquatic biological and bioinspired flow control strategies." *Communications Engineering* Vol. 2 No. 1 (2023): p. 30.
- [10] Videler, John J. Avian flight. Oxford University Press (2006).
- [11] Brown, R, Ferguson, J, Lawrence, M and Lees, D. "Tracks and Signs of the Birds of Britain and Europe: Christopher Helm." (1987).

- [12] Duan, Chengfang and Wissa, Aimy. "Covert-inspired flaps for lift enhancement and stall mitigation." *Bioinspiration & Biomimetics* Vol. 16 No. 4 (2021): p. 046020.
- [13] Meyer, Robert, Hage, Wolfram, Bechert, Dietrich W, Schatz, Markus, Knacke, Thilo and Thiele, Frank. "Separation control by self-activated movable flaps." *AIAA journal* Vol. 45 No. 1 (2007): pp. 191–199.
- [14] Bechert, D, Bruse, M, Hage, W, Meyer, R, Bechert, D, Bruse, M, Hage, W and Meyer, R. "Biological surfaces and their technological application-laboratory and flight experiments on drag reduction and separation control." 28th Fluid dynamics conference: p. 1960. 1997.
- [15] Bechert, DW, Bruse, M, Hage, W and Meyer, R. "Fluid mechanics of biological surfaces and their technological application." *Naturwissenschaften* Vol. 87 No. 4 (2000): pp. 157–171.
- [16] Brücker, Christoph and Weidner, Christoph. "Influence of self-adaptive hairy flaps on the stall delay of an airfoil in ramp-up motion." *Journal of Fluids and Structures* Vol. 47 (2014): pp. 31–40.
- [17] Duan, Chengfang, Waite, Josiah and Wissa, Aimy. "Design optimization of a covert feather-inspired deployable structure for increased lift." 2018 Applied Aerodynamics Conference: p. 3174. 2018.
- [18] Gardner, AD, Opitz, Steffen, Wolf, CC and Merz, Christoph B. "Reduction of dynamic stall using a back-flow flap." *CEAS Aeronautical Journal* Vol. 8 No. 2 (2017): pp. 271–286.
- [19] Wang, Longjun, Alam, Md Mahbub and Zhou, Yu. "Experimental study of a passive control of airfoil lift using bioinspired feather flap." *Bioinspiration & Biomimetics* Vol. 14 No. 6 (2019): p. 066005.
- [20] Fang, Zhe, Gong, Chunlin, Revell, Alistair, Chen, Gang, Harwood, Adrian and O'connor, Joseph. "Passive separation control of a NACA0012 airfoil via a flexible flap." *Physics of Fluids* Vol. 31 No. 10 (2019): p. 101904.
- [21] Nair, Nirmal J and Goza, Andres. "Fluid-structure interaction of a bio-inspired passively deployable flap for lift enhancement." *arXiv preprint arXiv:2203.00037* (2022).
- [22] Zekry, Diaa A, Nam, Taewoo, Gupta, Rikin, Zhu, Yufei and Wissa, Aimy A. "Covert-inspired flaps: an experimental study to understand the interactions between upperwing and underwing covert feathers." *Bioinspiration & Biomimetics* Vol. 18 No. 4 (2023): p. 046021.
- [23] Barlow, Jewel B, Rae, William H and Pope, Alan. *Low-speed wind tunnel testing*. John wiley & sons (1999).
- [24] Etkin, Bernard and Reid, Lloyd D. *Dynamics of flight*. Vol. 2. Wiley New York (1959).
- [25] Zekry, Diaa A, Duan, Chengfang, Ito, Mihary R and Wissa, Aimy A. "Design of experiments for two-and three-dimensional bio-inspired flow control devices." *AIAA Scitech 2021 Forum*: p. 0467. 2021.